01 May 2011

Forecasting the Cosmological Constraints with Anisotropic Baryon Acoustic Oscillations from Multipole Expansion

Atsushi Taruya

Shun Saito
Missouri University of Science and Technology, saitos@mst.edu

Takahiro Nishimichi

Follow this and additional works at: https://scholarsmine.mst.edu/phys_facwork

Part of the Physics Commons

Recommended Citation

Forecasting the cosmological constraints with anisotropic baryon acoustic oscillations from multipole expansion

Atsushi Taruya,[1,2] Shun Saito,[3] and Takahiro Nishimichi[2]

[1]*Research Center for the Early Universe, School of Science, The University of Tokyo, Bunkyo-ku, Tokyo 113-0033, Japan*
[2]*Institute for the Physics and Mathematics of the Universe, The University of Tokyo, Kashiwa, Chiba 277-8568, Japan*
[3]*Department of Astronomy, University of California Berkeley, California 94720, USA*

Baryon acoustic oscillations imprinted in the galaxy power spectrum can be used as a standard ruler to determine the angular diameter distance and Hubble parameter from high-redshift galaxies. Combining redshift distortion effect which apparently distorts the galaxy clustering pattern, we can also constrain the growth rate of large-scale structure formation. Usually, future forecasts for constraining these parameters from galaxy redshift surveys are made with the full 2D power spectrum characterized as a function of wave number k and directional cosine μ between line-of-sight direction and wave vector, i.e., $P(k, \mu)$. Here, we apply the multipole expansion to the full 2D power spectrum, and discuss how much cosmological information can be extracted from the lower-multipole spectra, taking a proper account of the nonlinear effects on gravitational clustering and redshift distortion. Fisher matrix analysis reveals that compared to the analysis with the full 2D spectrum, using only the partial information from the monopole and quadrupole spectra generally degrades the constraints by a factor of ~ 1.3 for each parameter. The additional information from the hexadecapole spectrum helps to improve the constraints, leading to a result that is almost comparable to the one expected from the full 2D spectrum.

I. INTRODUCTION

Baryon acoustic oscillations (BAOs) imprinted on the clustering of galaxies are now recognized as a powerful cosmological probe to trace the expansion history of the Universe [1–3]. In particular, the BAO measurement via a spectroscopic survey can provide a way to simultaneously determine the angular diameter distance D_A and Hubble parameter H at given redshift of galaxies through the cosmological distortion, known as the Alcock-Paczynski effect (e.g., [4–8]). Further, measuring the clustering anisotropies caused by the redshift distortion due to the peculiar velocity of galaxies, we can also probe the growth history of structure formation (e.g., [9–12]), characterized by the growth-rate parameter $f \equiv d \ln D / d \ln a$, with quantities D and a being linear growth factor and the scale factor of the Universe, respectively.

With the increased number of galaxies and large survey volumes, on-going and future spectroscopic galaxy surveys such as the Baryon Oscillation Spectroscopic Survey (BOSS) [13], Hobby-Eberly Dark Energy Experiment (HETDEX) [14], Subaru Measurement of Imaging and Redshift equipped with Prime Focus Spectrograph (SuMIRe-PFS), and EUCLID/JDEM [15,16] aim at precisely measuring the acoustic scale of BAOs as a standard ruler. These surveys will cover a wide redshift range, $0.3 \lesssim z \lesssim 3.5$, and provide a precise measurement of the redshift-space power spectrum with an accuracy of a percent level over the scales of BAOs.

In promoting these gigantic surveys, a crucial task is a quantitative forecast for the size of the statistical errors on the parameters D_A, H and f in order to clarify the scientific benefits as well as to explore the optimal survey design. The Fisher matrix formalism is a powerful tool to investigate these issues, and it enables us to quantify the precision and the correlation between multiple parameters ([5,7,17,18], especially for measuring D_A, H and f). So far, most of parameter forecast studies have focused on the potential power of the BAO measurements, and attempt to clarify the achievable level of precision for the parameter estimation. For this purpose, they sometimes assumed a rather optimistic situation that a full shape of the redshift-space power spectrum, including the clustering anisotropies due to the redshift distortion, is available in both observation and theory.

In this paper, we are particularly concerned with parameter estimation using partial information about the anisotropic BAOs from a practical point of view. In redshift space, the power spectrum obtained from spectroscopic measurements is generally described in two dimensions, and is characterized as a function of k and μ, where k is the wave number and μ is the directional cosine between line-of-sight direction and k [19]. While most of the forecast study is concerned with a full 2D power spectrum, the multipole expansion of the redshift-space power spectrum has been frequently used in the data analysis to quantify the clustering anisotropies. Denoting the power spectrum by $P(k, \mu)$, we have

$$P(k, \mu) = \sum_{\ell=0}^{\text{even}} P_\ell(k) \mathcal{P}_\ell(\mu), \tag{1}$$

with the function $\mathcal{P}_\ell$ being the Legendre polynomials. Although the analysis with the full 2D spectrum will definitely play an important role in improving the statistical signal, most of the recent cosmological data analysis has focused on the angle-averaged power spectrum ($\ell = 0$), i.e., the monopole spectrum, and a rigorous analysis with the full 2D spectrum is still a heavy task due to the time-consuming covariance estimation (e.g., [20–22]).

In linear theory, the redshift-space power spectrum is simply written as $P(k, \mu) = (1 + \beta\mu^2)^2 P_{\text{gal}}(k)$, where $\beta = f/b$ with b being the linear bias parameter, and P_{gal} is the galaxy power spectrum in real space [23–25]. Then, the nonvanishing components arise only from the monopole ($\ell = 0$), quadrupole ($\ell = 2$) and hexadecapole spectra ($\ell = 4$). That is, cosmological information contained in the $\ell = 0$, 2 and 4 moments is equivalent to the whole information in the full 2D power spectrum. Observationally, however, this is only the case when we know the cosmological distance to the galaxies *a priori*. The Alcock-Paczynski effect can induce nontrivial clustering anisotropies, which cannot be fully characterized by the lower-multipole spectra, in general. Further, in reality, a linear theory description cannot be adequate over the scale of the BAOs, and the nonlinear effects from redshift distortions as well as from the gravitational clustering must be considered for a proper comparison with observation. These facts imply that nonvanishing multipole spectra with $\ell > 4$ generically appear, and a part of the cosmological information might reside in those higher multipole moments. An important question is how much of the cosmological information can be robustly extracted from the lower-multipole spectra instead of the full 2D spectrum. In light of this, Ref. [8] recently examined a nonparametric method to constrain D_A and H from the monopole and quadrupole spectra, and numerically estimate the size of errors (see also Ref. [26] for the estimation of the growth-rate parameter).

Here, as a complementary and comprehensive approach, we will investigate this issue based on the Fisher matrix formalism, and derive useful formulae for parameter forecasts using the multipole power spectra. We then explore the potential power of the lower-multipole spectra for obtaining cosmological constraints, particularly focusing on the parameters D_A, H and f. To do so, we consider the figure-of-merit (FoM) and figure-of-bias (FoB) for these parameters, and investigate their dependence on the assumptions for the number density of galaxies, the amplitude of clustering bias, and the maximum wave number used for the parameter estimation.

In Sec. II, we present the Fisher matrix formalism for cosmological parameter estimation from the multipole power spectra. Section III deals with modeling of the redshift-space power spectrum and the assumptions used in the Fisher matrix analysis. Then, in Sec. IV, the results for the FoM and FoB are shown, and the sensitivity of the results to the assumptions and choice of the parameters is

discussed in greater detail. Finally, Sec. V briefly summarize our present work.

Throughout the paper, we assume a flat Lambda cold dark matter (CDM) model, and the fiducial model parameters are chosen based on the five-year WMAP results [27]: $\Omega_m = 0.279$, $\Omega_\Lambda = 0.721$, $\Omega_b = 0.0461$, $h = 0.701$, $n_s = 0.96$, $A_s = 2.19 \times 10^{-9}$.

II. FISHER MATRIX FORMALISM

In this section, we present the basic formulae for Fisher matrix analysis in estimating the statistical error and systematic biases for cosmological parameters from the multipole power spectra.

Let us first derive the expression for the Fisher matrix relevant for power spectrum analysis. The definition of the Fisher matrix is given by

$$F_{ij} = -\left\langle \frac{\partial^2 \ln \mathcal{L}}{\partial\theta_i \partial\theta_j} \right\rangle, \qquad (2)$$

where θ_i denotes the parameter, and the quantity $\mathcal{L}$ is the likelihood function. For the parameter estimation study with the multipole spectrum, $P_\ell(k)$, the likelihood function is usually taken to be the form

$$\mathcal{L} \propto \exp\left[-\frac{1}{2} \sum_{m,n} \sum_{\ell,\ell'} \Delta P_\ell(k_m) [C^{\ell\ell'}(k_m, k_n)]^{-1} \Delta P_{\ell'}(k_n) \right], \qquad (3)$$

where we define

$$\Delta P_\ell(k) \equiv \hat{P}_\ell(k) - P_\ell(k),$$
$$C^{\ell\ell'}(k_m, k_n) \equiv \langle \Delta P_\ell(k_m) \Delta P_{\ell'}(k_n) \rangle.$$

The quantities $\hat{P}_\ell(k)$ and $P_\ell(k)$ respectively denote the observed estimate and theoretical template for the multipole power spectrum.

Substituting Eq. (3) into the definition (2), the leading-order evaluation of the Fisher matrix leads to (e.g., [28,29]):

$$F_{ij} \simeq \sum_n \sum_{\ell,\ell'} \frac{\partial P_\ell(k_n)}{\partial\theta_i} [\text{Cov}^{\ell\ell'}(k_n)]^{-1} \frac{\partial P_\ell(k_n)}{\partial\theta_j}, \qquad (4)$$

where we have assumed that the covariance is approximately characterized by Gaussian statistics and is written as $C^{\ell\ell'}(k_m, k_n) = \text{Cov}^{\ell\ell'}(k_n)\delta_{mn}$, where δ_{mn} is the Kronecker symbol.

Adopting the power spectrum estimation of Ref. [30], the analytic expression for the quantity $\text{Cov}^{\ell\ell'}(k_n)$ can be found in Ref. [31] [see Eq. (25) of their paper]:

$$\text{Cov}^{\ell\ell'}(k_n) = \frac{2}{V_n} \frac{(2\ell + 1)(2\ell' + 1)}{2}$$
$$\times \int_{-1}^1 d\mu \frac{\mathcal{P}_\ell(\mu)\mathcal{P}_{\ell'}(\mu)}{\int d^3 r \bar{n}(r)^2 [1 + \bar{n}(r)P^{(S)}(k_n, \mu)]^{-2}} \qquad (5)$$

with $\mathcal{P}_\ell(\mu)$ being the Legendre polynomial [32]. The quantity V_n is the volume element of a thin shell in Fourier space, i.e., $V_n = 4\pi^2 k_n^2 dk_n/(2\pi)^3$, which corresponds to $\Delta V_k/(2\pi)^3$ in the notation of Ref. [31].

Now, to simplify the formula, we consider homogeneous galaxy samples, which implies $\bar{n}(r) = \bar{n} = $ const. In this case, the denominator in the integrand of Eq. (5) is simplified as

$$\int d^3 r \, \bar{n}(r)^2 [1 + \bar{n}(r) P(k, \mu)]^{-2} = V_s \left\{ P(k, \mu) + \frac{1}{\bar{n}} \right\}^{-2}, \quad (6)$$

where V_s denotes the survey volume. Then, taking the continuum limit, the expression for the Fisher matrix can be recast as

$$F_{ij} = \frac{V_s}{4\pi^2} \int_{k_{\min}}^{k_{\max}} dk k^2 \sum_{\ell, \ell'} \frac{\partial P_\ell(k)}{\partial \theta_i} [\widetilde{\mathrm{Cov}}^{\ell\ell'}(k)]^{-1} \frac{\partial P_\ell(k)}{\partial \theta_j}, \quad (7)$$

with the reduced covariance matrix $\widetilde{\mathrm{Cov}}^{\ell\ell'}(k)$ given by

$$\widetilde{\mathrm{Cov}}^{\ell\ell'}(k) = \frac{(2\ell + 1)(2\ell' + 1)}{2} \int_{-1}^{1} d\mu \, \mathcal{P}_\ell(\mu) \mathcal{P}_{\ell'}(\mu)$$
$$\times \left[P(k, \mu) + \frac{1}{\bar{n}} \right]^2. \quad (8)$$

Here, the range of integration $[k_{\min}, k_{\max}]$ should be chosen through the survey properties and/or limitation of the theoretical template, and, in particular, the minimum wave number is limited to $2\pi/V_s^{1/3}$.

Equation (7) with (8) is the formula for the Fisher matrix used in the parameter estimation with multipole power spectra. This can be compared with the standard formula for the full 2D power spectrum (e.g., [5,7,29]):

$$F_{ij}^{(2D)} = \frac{V_s}{4\pi^2} \int_{k_{\min}}^{k_{\max}} dk k^2 \int_{-1}^{1} d\mu \frac{\partial P(k, \mu)}{\partial \theta_i} \left\{ P(k, \mu) + \frac{1}{\bar{n}} \right\}^{-2}$$
$$\times \frac{\partial P(k, \mu)}{\partial \theta_j} \quad (9)$$

That is, the full 2D information obtained through the integral over the directional cosine μ in Eq. (9) is replaced with a summation over all multipoles in the new formula (7). Thus, truncating the summation at a lower multipole generally leads to the reduction of the amplitude in the Fisher matrix, and as a result, the statistical errors of the parameter θ_i marginalized over other parameters, given by $\Delta\theta_i = \sqrt{\{F^{-1}\}_{ii}}$, is expected to become larger.

The Fisher matrix formalism also provides a simple way to estimate the biases in the best-fit parameters caused by an incorrect template for the multipole power spectra $P_\ell^{\mathrm{wrong}}(k)$. To derive the formula for systematic bias, we replace the template power spectrum $P_\ell(k)$ in the likelihood function (3) with the incorrect one $P_\ell^{\mathrm{wrong}}(k)$. We denote this likelihood function by $\mathcal{L}'$. Assuming that the size of the biases are basically small, the (biased) best-fit

values can be estimated from the extremum of the Likelihood function $\mathcal{L}'$ by expanding the expression of the extremum around the fiducial parameters:

$$0 = \frac{\partial \ln \mathcal{L}'}{\partial \theta_j} \simeq \frac{\partial \ln \mathcal{L}'}{\partial \theta_j} \bigg|_{\mathrm{fid}} + \sum_i \frac{\partial \ln \mathcal{L}'}{\partial \theta_i \partial \theta_j} \bigg|_{\mathrm{fid}} \delta\theta_i, \quad (10)$$

where the quantities with subscript $_{\mathrm{fid}}$ stand for the one evaluated at the fiducial parameters, and the $\delta\theta_i$ means the deviation of the best-fit value from the fiducial parameter. Then, taking the ensemble average of the above expressions and using the definition of the Fisher matrix, we obtain

$$\delta\theta_i = -\sum_j (F')_{ij}^{-1} s_j, \quad (11)$$

where the Fisher matrix F'_{ij} is the same one as given by Eq. (7), but is evaluated using incorrect power spectra $P_\ell^{\mathrm{wrong}}(k)$. The vector s_j is

$$s_j = \frac{V_s}{4\pi^2} \int_{k_{\min}}^{k_{\max}} dk k^2 \sum_{\ell, \ell'} P_\ell^{\mathrm{sys}}(k) [\widetilde{\mathrm{Cov}}^{\ell\ell'}(k)]^{-1} \frac{\partial P_{\ell'}^{\mathrm{wrong}}(k)}{\partial \theta_j}. \quad (12)$$

Here, the multipole power spectrum $P_\ell^{\mathrm{sys}}(k)$ denotes the systematic difference between the correct and incorrect models of the multipole power spectra, $P_\ell^{\mathrm{sys}}(k) = P_\ell^{\mathrm{wrong}}(k) - P_\ell^{\mathrm{true}}(k)$. In deriving the above expression, we have used the fact that the extremum of the likelihood function is obtained only when the correct template for the multipole power spectrum is applied.

Notice that a similar but essentially different formula for systematic biases is obtained when using the full 2D power spectrum. It is formally expressed as Eq. (11), but the Fisher matrix F'_{ij} is now replaced with Eq. (9) evaluated using the incorrect 2D spectrum $P^{\mathrm{wrong}}(k, \mu)$. Further, the vector s_j should be replaced with the one for the full 2D spectrum (e.g., [33,34]):

$$s_j^{(2D)} = \frac{V_s}{4\pi^2} \int_{k_{\min}}^{k_{\max}} dk k^2 \int_{-1}^{1} d\mu P^{\mathrm{sys}}(k, \mu)$$
$$\times \left[P_{\ell'}^{\mathrm{wrong}}(k, \mu) + \frac{1}{\bar{n}_g} \right]^{-2} \frac{\partial P^{\mathrm{wrong}}(k, \mu)}{\partial \theta_j}. \quad (13)$$

Finally, all the formulae derived in this section ignore non-Gaussian contributions to the likelihood and covariances, which would become practically important in some cases. In particular, the mode-coupling due to the gravitational clustering not only increases the amplitude $\mathrm{Cov}^{\ell\ell'}(k)$, but also produces a nontrivial correlation between different Fourier modes, leading to a nonvanishing off-diagonal component in the covariance matrices, i.e., $C^{\ell\ell'}(k_m, k_n) \neq 0$ for $k_m \neq k_n$ (e.g., [35]). Obviously, these two effects degrade the parameter constraints, and the forecast study based on the Gaussian Fisher matrix would be certainly optimistic. Interestingly, however, the impact

of the non-Gaussian errors is shown to be mitigated in the case of multiparameter estimation due to severe parameter degeneracies in the power spectrum [36–38]. Thus, in some cases, the Gaussian Fisher matrix can provide a good approximation for parameter forecast, and the formalism presented here is useful in quantitatively estimating the size of statistical errors. For more details on the role of the non-Gaussian contribution especially focusing on BAOs, see Refs. [21,36,39].

III. MODEL AND ASSUMPTIONS

Given the formulae for Fisher matrix analysis, we now move to the discussion on the parameter forecast study using the multipole power spectra, and compare the results with those obtained from the full 2D spectrum. Before doing this, in this section, we briefly describe the model and assumptions for the redshift-space power spectrum relevant for spectroscopic measurement of BAOs.

In redshift-space, clustering statistics generally suffer from two competing effects, i.e., enhancement and suppression of clustering amplitude, referred to as the Kaiser and Finger-of-God effects, respectively. While the Kaiser effect comes from the coherent motion of matter (or galaxies), the Finger-of-God effect is mainly attributed to the virialized random motion of the mass residing at a halo. In the weakly nonlinear regime, a tight correlation between velocity and density fields still remains, and a mixture of Kaiser and Finger-of-God effects is expected to be significant. Thus, a careful treatment is needed for accurately modeling the anisotropic power spectrum.

Recently, we have presented an improved prescription for the matter power spectrum in redshift space taking account of both nonlinear clustering and redshift distortions [34]. Based on the perturbation theory calculation, the model can give an excellent agreement with the results of N-body simulations, and a percent-level precision is almost achieved over the scales of interest for BAOs. The full 2D power spectrum of this model is very similar to the one proposed by Ref. [40], but includes corrections:

$$P(k, \mu) = e^{-(k\mu f \sigma_v)^2}\{P_{\delta\delta}(k) + 2f\mu^2 P_{\delta\theta}(k)$$
$$+ f^2\mu^4 P_{\theta\theta}(k) + A(k, \mu; f) + B(k, \mu; f)\} \quad (14)$$

with the quantity f being the growth-rate parameter. Here, the power spectra $P_{\delta\delta}$, $P_{\theta\theta}$ and $P_{\delta\theta}$ denote the auto power spectra of density and velocity divergence, and their cross power spectrum, respectively. The velocity divergence θ is defined by $\theta \equiv -\nabla v/(aHf)$. The quantity σ_v denotes the one-dimensional velocity dispersion [41], and the exponential prefactor characterizes the damping behavior by the Finger-of-God effect. For the purpose of modeling the shape and structure of BAOs in the power spectrum, σ_v may be treated as a free parameter, and determined by fitting the predictions to the observations.

A salient property of the model (14) is the presence of the terms A and B, which represent the higher-order couplings between velocity and density fields, usually neglected in phenomenological models of redshift distortions. The explicit expressions for these terms are derived based on the standard treatment of perturbation theory, and the results are presented in Ref. [34]. A detailed investigation in our previous paper [34] reveals that the corrections A and B can give an important contribution to the acoustic structure of BAOs over the scales $k \sim 0.2h$ Mpc^{-1}, which gives rise to a slight increase in the amplitude of the monopole and quadrupole spectra. With the improved treatment of perturbation theory to compute $P_{\delta\delta}$, $P_{\theta\theta}$ and $P_{\delta\theta}$ (e.g., [42,43]), the model (14) can give a better prediction than other current models of redshift distortions. Figure 1 plots the illustrated example showing that the model (14) reproduces the N-body results of the monopole
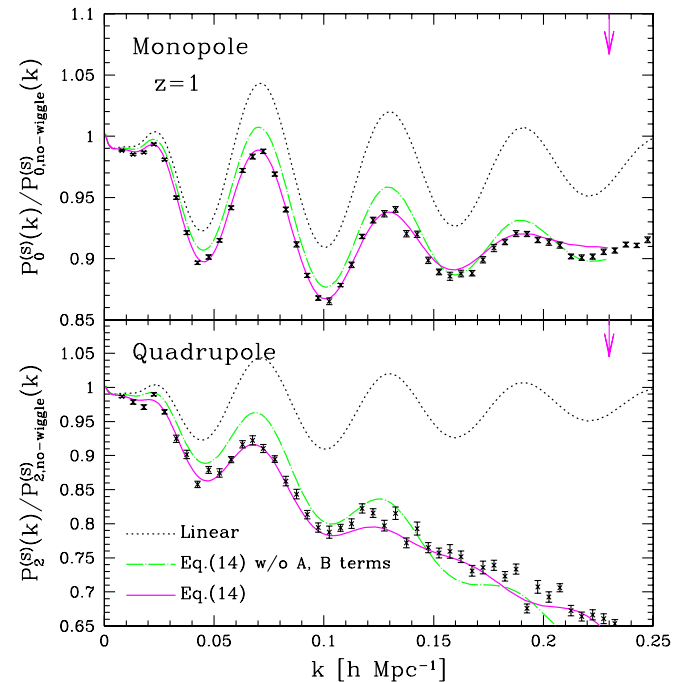

FIG. 1 (color online). Monopole (top) and quadrupole (bottom) moments of the matter power spectrum in redshift space at $z = 1$. The results are divided by the smooth reference spectrum, $P^{(S)}_{\ell,\text{no-wiggle}}$, and are compared with the N-body results (symbols) taken from the WMAP5 simulations of Ref. [42]. The reference spectrum $P^{(S)}_{\ell,\text{no-wiggle}}$ is calculated from the no-wiggle approximation of the linear transfer function [54] with the linear theory of the Kaiser effect taken into account. Solid and dash-dotted lines represent the results of improved PT calculations based on the model of redshift distortion (14), but the terms A and B are ignored in the dash-dotted lines. In both cases, the one-dimensional velocity dispersion σ_v was determined by fitting the predictions to the N-body simulations, using the data below the wave number indicated by the vertical arrow. The best-fit values of σ_v are $\sigma_v = 395$ km s^{-1} and 285 km s^{-1}, with and without the A and B terms, respectively.

and quadrupole spectra quite well, and the precision of the agreement between prediction and simulation reaches a percent-level. Hence, in this paper, we adopt the model (14) as a fiducial model for the matter power spectrum in redshift space.

Note that the model (14) generically produces nonvanishing higher multipole spectra for $\ell > 4$, due to the damping factor, $e^{-(k\mu f\sigma_v)^2}$. Furthermore, the corrections A and B are expanded as a power series of μ, which include the powers up to μ^6 for the A term, μ^8 for the B term. This indicates that the corrections additionally contribute to the higher multipoles, at least, up to $\ell = 8$. In this sense, the model (14) provides an interesting testing ground to estimate the extent to which the useful cosmological information can be obtained from the lower-multipole spectra.

Then, assuming a linear galaxy bias in real space, $\delta_{\mathrm{gal}} = b\delta_{\mathrm{mass}}$, the redshift-space power spectrum for galaxies becomes

$$P_{\mathrm{gal}}(k, \mu) = e^{-(k\mu f\sigma_v)^2} b^2 \{P_{\delta\delta}(k) + 2\beta\mu^2 P_{\delta\theta}(k) \\ + \beta^2 \mu^4 P_{\theta\theta}(k) + bA(k, \mu; \beta) + b^2 B(k, \mu; \beta)\} \tag{15}$$

with $\beta = f/b$. The linear deterministic bias may be too simplistic of an assumption, and the effects of nonlinearity and stochasticity in the galaxy bias might be non-negligible [44–46]. Our primary concern here is the qualitative aspects of parameter estimation using the multipole spectra, based on a physically plausible model of redshift distortions. Since the galaxy bias itself does not produce additional clustering anisotropies, we simply adopt the linear bias relation for illustrative purposes.

Finally, notice that in addition to the clustering anisotropies caused by the peculiar velocity of galaxies, the observed galaxy power spectrum defined in comoving space further exhibits anisotropies induced by the Alcock-Paczynski effect. This is modeled as

$$P_{\mathrm{obs}}(k, \mu) = \frac{H(z)}{H_{\mathrm{fid}}(z)} \left[\frac{D_{A,\mathrm{fid}}(z)}{D_A(z)}\right]^2 P_{\mathrm{gal}}(q, \nu), \tag{16}$$

where the quantity $P_{\mathrm{gal}}(q, \nu)$ at the right-hand side represents the template for the redshift-space power spectrum in the absence of cosmological distortion, i.e., Eq. (15). The comoving wave number k and the directional cosine μ measured with the underlying cosmological model are related to the true ones q and ν by the Alcock-Paczynski effect through (e.g., [8,47,48])

$$q = k\left[\left(\frac{D_{A,\mathrm{fid}}}{D_A}\right)^2 + \left\{\left(\frac{H}{H_{\mathrm{fid}}}\right) - \left(\frac{D_{A,\mathrm{fid}}}{D_A}\right)^2\right\}\mu^2\right]^{1/2}, \tag{17}$$

$$\nu = \left(\frac{H}{H_{\mathrm{fid}}}\right)\mu\left[\left(\frac{D_{A,\mathrm{fid}}}{D_A}\right)^2 + \left\{\left(\frac{H}{H_{\mathrm{fid}}}\right) - \left(\frac{D_{A,\mathrm{fid}}}{D_A}\right)^2\right\}\mu^2\right]^{-1/2}, \tag{18}$$

The quantities $D_{A,\mathrm{fid}}$ and H_{fid} are the fiducial values of the angular diameter distance and Hubble parameter at a given redshift slice.

IV. RESULTS

In what follows, for illustrative purposes, we consider a hypothetical galaxy survey of volume $V_s = 4h^{-3}$ Gpc^3 at $z = 1$, and examine how well we can constrain the distance information and growth-rate parameter, D_A, H, and f, from the low-multipole power spectra. We set the number density of galaxies, linear bias parameter and velocity dispersion to $\bar{n} = 5 \times 10^{-4} h^3$ Mpc-3, $b = 2$ and $\sigma_v = 395$ km s^{-1}. These values are used in the Fisher analysis as a canonical setup, but we also examine the effect of varying this parameter set to study the sensitivity of the forecast results. Note that the depth and the volume of the survey considered here roughly match those of a stage III-class survey defined by the Dark Energy Task Force (DETF) [49].

To compute the Fisher matrix adopting the model of the redshift-space power spectrum, Eq. (15), we just follow the procedure in Ref. [34] to calculate the redshift-space power spectra. That is, we use the improved perturbation theory (PT) developed by Refs. [42,50] to account for a dominant contribution of the nonlinear gravity to the power spectra $P_{\delta\delta}$, $P_{\delta\theta}$ and $P_{\theta\theta}$, and to adopt standard PT for small but non-negligible corrections of A and B terms. Detailed comparison with N-body simulations [34,42] showed that this treatment can work well, and in our fiducial set of cosmological parameters, the model can give a percent-level precision at least up to the wave number $k \leq 0.2h$ Mpc^{-1} at $z = 1$.

The number of free parameters in the subsequent Fisher analysis is five in total, i.e., D_A, H, and f, in addition to the parameters b and σ_v. Other cosmological parameters such as Ω_m or Ω_b are kept fixed. We assume that the cosmological model dependence of the power spectrum shape is perfectly known *a priori* from the precision cosmic microwave background (CMB) measurement by Planck [51]. The influence of the uncertainty in the power spectrum shape is discussed in Sec. IV C 2 in detail.

A. Two-dimensional errors

As a pedagogical example, let us first examine how the lower-multipole spectra can constrain the parameters D_A, H, and f. Figure 2 shows the two-dimensional contour of the 1–σ (68% C.L.) errors on (D_A, H) (bottom left), (D_A, f) (top left), and (f, H)-planes (bottom right). Here, the Fisher matrix is computed adopting the model of redshift-space power spectrum (15) up to $k_{\mathrm{max}} = 0.2h$ Mpc^{-1}.

The magenta solid and cyan dashed lines, respectively, represent the constraints coming from the monopole (P_0) and quadrupole (P_2) power spectrum alone. As anticipated, a single multipole by itself cannot provide useful
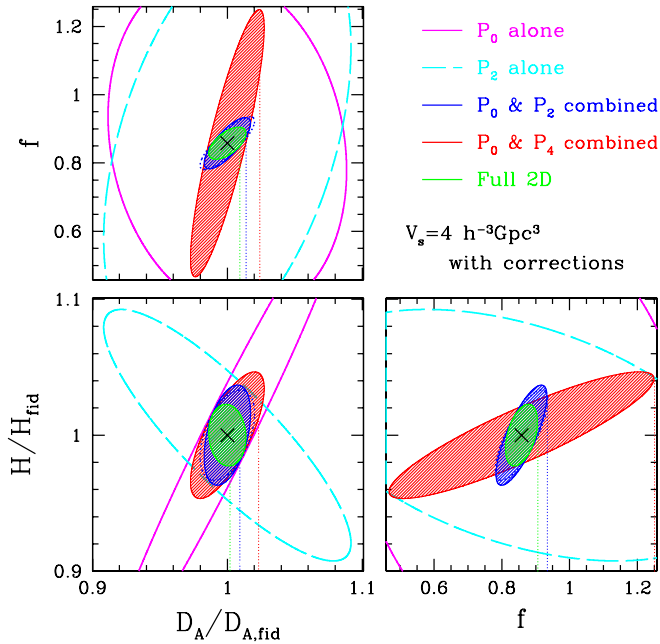
FIG. 2 (color online). Two-dimensional contours of 1-σ (68% C.L.) errors on (D_A, H) (bottom left), (D_A, f) (top left), and (f, H) (bottom right), assuming a stage-III-class survey with $V_s = 4h^{-3}\text{Gpc}3$ at $z = 1$. In each panel, magenta solid and cyan dashed lines, respectively, indicate the forecast constraints coming from the monopole (P_0) and quadrupole (P_2) spectrum alone, while the middle and outer shaded regions (indicated by blue and red online) represent the combined constraints from P_0 and P_2, and P_0 and P_4, respectively. The innermost shaded region (indicated by green online) represents the results coming from the full 2D spectrum. As a reference, blue dotted contours show the results combining both P_0 and P_2, but (incorrectly) neglecting the covariance between monopole and quadrupole spectra, i.e., $\widetilde{\text{Cov}}^{02} = \widetilde{\text{Cov}}^{20} = 0$.

information to simultaneously constrain D_A, H, and f. In particular, for the constraints on D_A and H, there appear strong degeneracies, and the error ellipses are highly elongated and inclined. These behaviors are basically deduced from the Alcock-Paczynski effect, and are consistent with the facts that the monopole spectrum is rather sensitive to the combination (D_A^2/H), while the quadrupole spectrum is sensitive to $(D_A H)$ (e.g., [8]). On the other hand, combining the monopole and quadrupole greatly improves the constraints (indicated by the blue, outer shaded region) not only on D_A and H, but also on growth-rate parameter f. This is because the degeneracies between the parameters D_A and H constrained by the monopole differ from that by the quadrupole, and thus the combination of these two spectra leads to a substantial reduction of the size of error ellipses. Further, the growth-rate parameter is proportional to the strength of redshift distortions, and can be determined by the quadrupole-to-monopole ratio. Although the measurement of the galaxy power spectrum alone merely gives a constraint on $\beta = f/b$, provided an accurate CMB measurement of the power spectrum normalization, we can

separately determine the growth-rate parameter. Note that the combination of the monopole and hexadecapole spectra also provides a way to determine the growth-rate parameter (red shaded region), although the error on f is a bit larger due to the small amplitude of the hexadecapole spectrum.

For comparison, Fig. 2 also shows the forecast constraints obtained from the full 2D power spectrum (green, inner shaded region). Further, we plot the results of combining the monopole and quadrupole spectra, but neglecting the covariance between $\ell = 0$ and $\ell = 2$, i.e., $\widetilde{\text{Cov}}^{02} = \widetilde{\text{Cov}}^{20} = 0$ (blue, dotted lines). Clearly, using the full 2D shape of the redshift-space power spectrum leads to a tighter constraint, and the area of the two-dimensional error is reduced by a factor of 1.6–18, compared with the constraints from the monopole and quadrupole spectra. These results indicate that the contribution of the higher multipoles is very important, and the additional information from the quadrupole and hexadecapole spectra, each of which puts a different direction of parameter degeneracies, seems to play a dominant role in improving the constraints. On the other hand, for joint constraints from the monopole and quadrupole, the role of the covariance $\widetilde{\text{Cov}}^{02}$ or $\widetilde{\text{Cov}}^{20}$ seems less important, and one may naively treat the monopole and quadrupole power spectra as statistically independent quantities. However, these results are partially due to the properties of the galaxy samples characterized by several parameters, and may be altered with different assumptions or survey setup. This point will be investigated in some detail in the next subsection.

B. Figure-of-Merit

We here study the dependence of galaxy samples or survey setup on the forecast results for parameter constraints. To do this, it is useful to define the figure-of-merit :

$$\text{FoM} \equiv \frac{1}{\sqrt{\det \widetilde{\boldsymbol{F}}^{-1}}}, \qquad (19)$$

where the matrix $\widetilde{\boldsymbol{F}}^{-1}$ is the 3×3 submatrix, whose elements are taken from the inverse Fisher matrix $\boldsymbol{F} - 1$ associated with the parameters D_A, H, and f. The FoM quantifies the improvement of the parameter constraints, and is inversely proportional to the product of one-dimensional marginalized errors, i.e., $\text{FoM} \propto 1/\{\sigma(D_A)\sigma(H)\sigma(f)\}$.

Figure 3 shows the dependence of the FoM on the properties of the galaxy samples characterized by the number density n_g (top right), bias parameter b (bottom left), and one-dimensional velocity dispersion σ_v (bottom right). Also, in the top left panel, we show the FoM as a function of the maximum wave number k_{max} used in the parameter estimation study. Note that in plotting the results, the other parameters are kept fixed to the canonical values. The upper part of each panel plots the three different lines, and shows how the FoM changes depending on
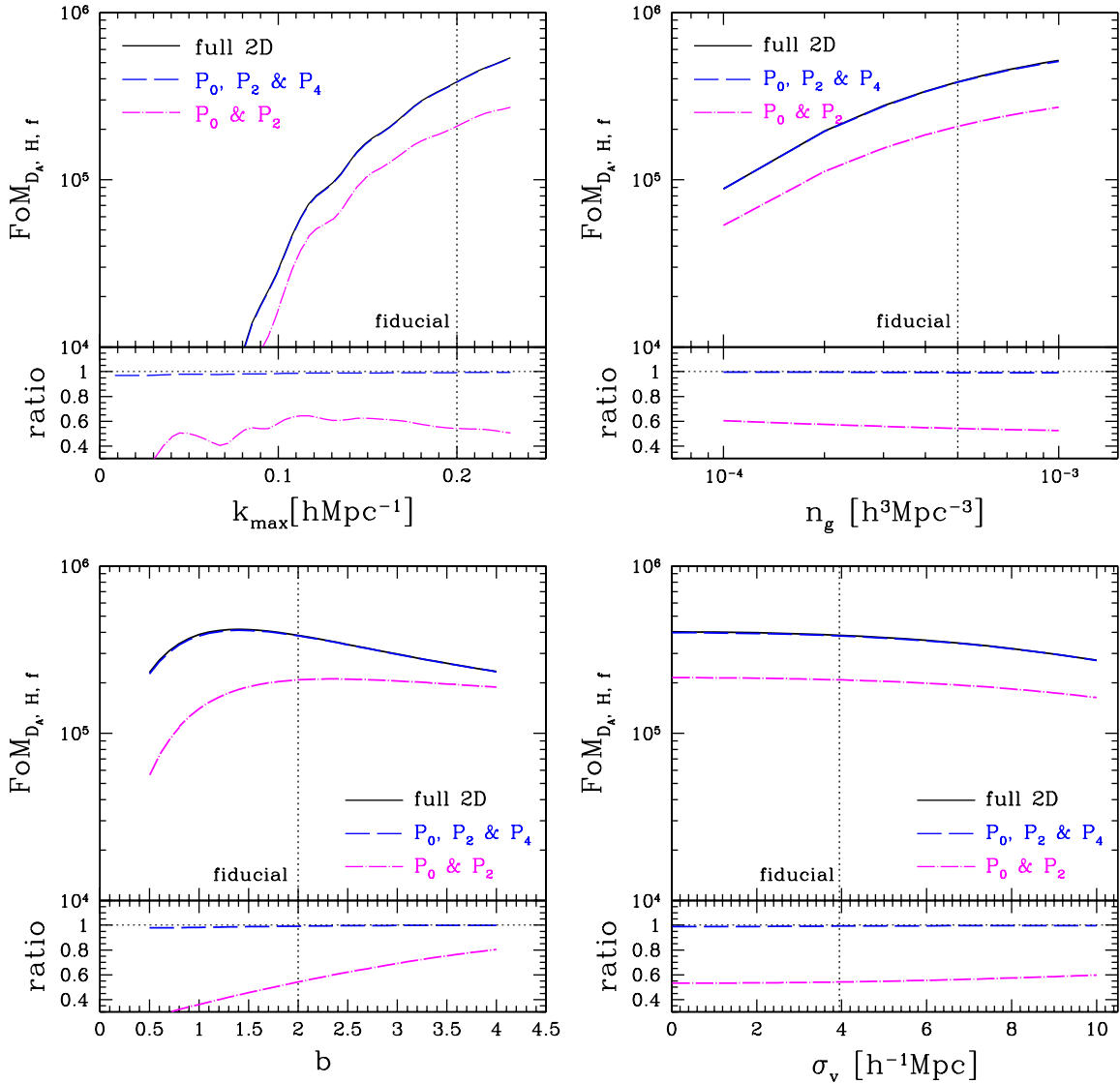
FIG. 3 (color online).   Figure-of-merit for the parameters D_A, H, and f defined by Eq. (19), as functions of k_{max} (top left), $\bar{n}_{gal}$ (top right), b (bottom left), and σ_v (bottom right), assuming a hypothetical galaxy survey at $z = 1$ with volume $V_s = 4h^{-3}$ Gpc^3. In each panel, solid lines are the results obtained from the full 2D power spectrum, while the dashed and dash-dotted lines represent the FoM from the combination of the multipole spectra (dash-dotted: P_0 & P_2, dashed: P_0, P_0, & P_4). The bottom panels show the ratio of FoM normalized by the one obtained from the full 2D spectrum. Note that except for the parameter along the horizontal axis, the fiducial values of the model parameters are set to $k_{max} = 0.2h$ Mpc^{-1}, $n_g = 5 \times 10^{-4}h^3$ Mpc^{-3}, $b = 2$, and $\sigma_v = 3.95h^{-1}$ Mpc, indicated by the vertical dotted lines.

the choice or combination of power spectra used in the analysis: combining monopole (P_0) and quadrupole (P_2) spectra (magenta, dash-dotted); combining three multipole spectra, P_0, P_2 and P_4 (blue, long dashed); using the full 2D spectrum $P(k, \mu)$ (black, solid). On the other hand, the lower part of each panel plots the ratio of FoM normalized by the one for the full 2D spectrum.

In principle, using the full 2D spectrum gives the tightest constraints on D_A, H, and f, but an interesting point here is that a nearly equivalent FoM to the one for the full 2D spectrum is obtained even from partial information with the lower-multipole spectra P_0, P_2 and P_4. This is irrespective of the choice of the parameters for galaxy samples.

Although the result may rely on the model of redshift distortions adopted in this paper, recalling the fact that the nonvanishing multipole spectra higher than $\ell \gtrsim 6$ arise only from the nonlinear effects through the gravitational evolution and redshift distortion, the cosmological model dependence encoded in these higher multipoles is expected to be very weak, partly due to the low signal-to-noise ratio. In this sense, the result in Fig. 3 seems reasonable.

Now, we focus on the FoM from the combination of P_0 and P_2. Figure 3 indicates that except for the case varying the bias b, the resultant FoM shows a monotonic dependence on the parameters. As a result, the ratio of FoM shown in the lower part of the panels is nearly constant

around 0.4–0.6. As for the variation of the bias parameter, the nonmonotonic dependence of the FoM is basically explained by the competition between two effects. That is, for increasing b, while the power spectrum amplitude increases and signal-to-noise ratio is enhanced, the clustering anisotropies due to the redshift distortion controlled by the quantity β are gradually reduced. Hence, for some values of b, FoM becomes maximum. A noticeable point is that the ratio of FoM for the monopole and quadrupole gradually increases as the clustering bias becomes large. At $b \sim 4$, the ratio of FoM reaches at 0.8, indicating most of the cosmological information contained in the hexadeca-pole and higher multipoles is lost, and the signal coming from the monopole and quadrupole spectra becomes dominant.

The reason for this behavior is presumably due to the covariance between the multipole spectra, $\widetilde{\mathrm{Cov}}^{\ell\ell'}$. In the linear regime, the covariance neglecting the shot-noise contribution is determined by the galaxy power spectrum in real space and the parameter $\beta = f/b$, and the off-diagonal component $\widetilde{\mathrm{Cov}}^{02} = \widetilde{\mathrm{Cov}}^{20}$ is roughly proportional to β. Thus, increasing the clustering bias b while keeping the growth-rate parameter fixed, the covariance $\widetilde{\mathrm{Cov}}^{02}$ becomes smaller, and the monopole and quadrupole power spectra become statistically independent. To see this more explicitly, we define

$$r_{\mathrm{cov}} = \frac{\widetilde{\mathrm{Cov}}^{0,2}}{[\widetilde{\mathrm{Cov}}^{0,0}\widetilde{\mathrm{Cov}}^{2,2}]^{1/2}}. \tag{20}$$

In Fig. 4, taking account of the shot-noise contribution, the quantity r_{cov} is plotted against the parameter β. Here,
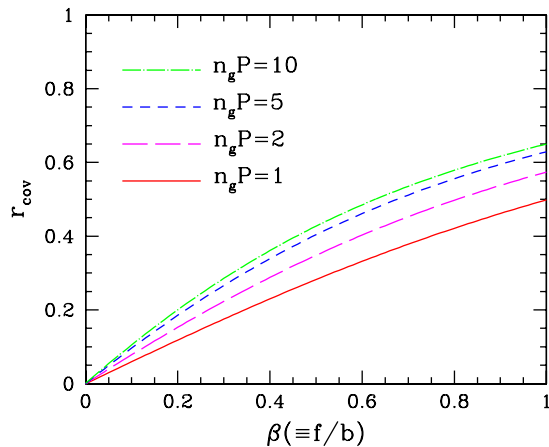

FIG. 4 (color online).   Correlation coefficient for the covariance, $r_{\mathrm{cov}} = \widetilde{\mathrm{Cov}}^{0,2}/[\widetilde{\mathrm{Cov}}^{0,0}\widetilde{\mathrm{Cov}}^{2,2}]^{1/2}$, as a function of $\beta \equiv f/b$. The plotted results are obtained based on the linear theory, in which the coefficient r_{cov} depends on the power spectrum amplitude relative to the shot-noise contribution, $n_{\mathrm{g}}P$, as well as β. The solid, long-dashed, short-dashed, and dash-dotted lines, respectively, indicate the results with $n_{\mathrm{g}}P = 1$, 2, 5, and 10.

we used the linear theory to calculate $\widetilde{\mathrm{Cov}}^{\ell\ell'}$. Figure 4 implies that in our fiducial setup with $f = 0.858$, r_{cov} becomes $\lesssim 0.2$ for the bias $b = 4$. Since the smaller values of β also suppress the Kaiser effect in the covariances $\widetilde{\mathrm{Cov}}^{00}$ and $\widetilde{\mathrm{Cov}}^{22}$, the constraints from the monopole and quadrupole spectra are relatively improved.

This result suggests that even the partial information with monopole and quadrupole spectra still provides a fruitful constraint on D_A, H and f, depending on the survey setup. In this respect, a benefit to use these power spectra should be further explored. As a next step, we will discuss the robustness of the parameter constraints against systematic biases.

C. Impact of systematic biases

Among various possible systematics that affect the parameter constraints, the incorrect assumption for the theoretical template of power spectra may seriously lead to a bias in the best-fit parameters. There are several routes to produce an incorrect theoretical template; incorrect modeling of redshift distortions and/or nonlinear gravitational evolution, wrong prior information for cosmological parameters, or improper parametrization for galaxy bias. In this subsection, we specifically examine the first and second cases. We first discuss the incorrect model of redshift distortion, and quantify the size of the systematic bias in the best-fit parameter. The effect of using the wrong prior information will be discussed in the next subsection.

1. Systematic biases from a wrong model of redshift distortion

Let us first discuss the impact of assuming an incorrect model of redshift distortions on the parameter estimation. To be precise, we consider the small discrepancy in the theoretical template for the redshift-space power spectrum (15), and estimate the systematic biases from Eq. (11). Figure 5 shows the systematic biases caused by the incorrect model template neglecting the A and B terms. We plot the results by varying the model parameters, $k_{\max}$ (top left), n_{g} (top right), b (bottom left), and σ_{v} (bottom right), around the fiducial values. In each panel, the first three plots from the top show the deviation of the best-fit value from the fiducial one, δf, δD_A, and δH, normalized by their fiducial values. On the other hand, the lowest panel shows the figure-of-bias , which represents the statistical significance of systematic biases relative to the statistical errors, defined by [52,53]:

$$\mathrm{FoB} \equiv \left(\sum_{i,j}\delta\theta_i \widetilde{F}'_{ij}\delta\theta_j\right)^{1/2}. \tag{21}$$

Note that the matrix $\widetilde{F}'_{ij}$ is the same inverse of the sub-matrix $\widetilde{F}^{-1}_{ij}$ as defined in Eq. (19), but with the Fisher matrix obtained from the incorrect template. With the
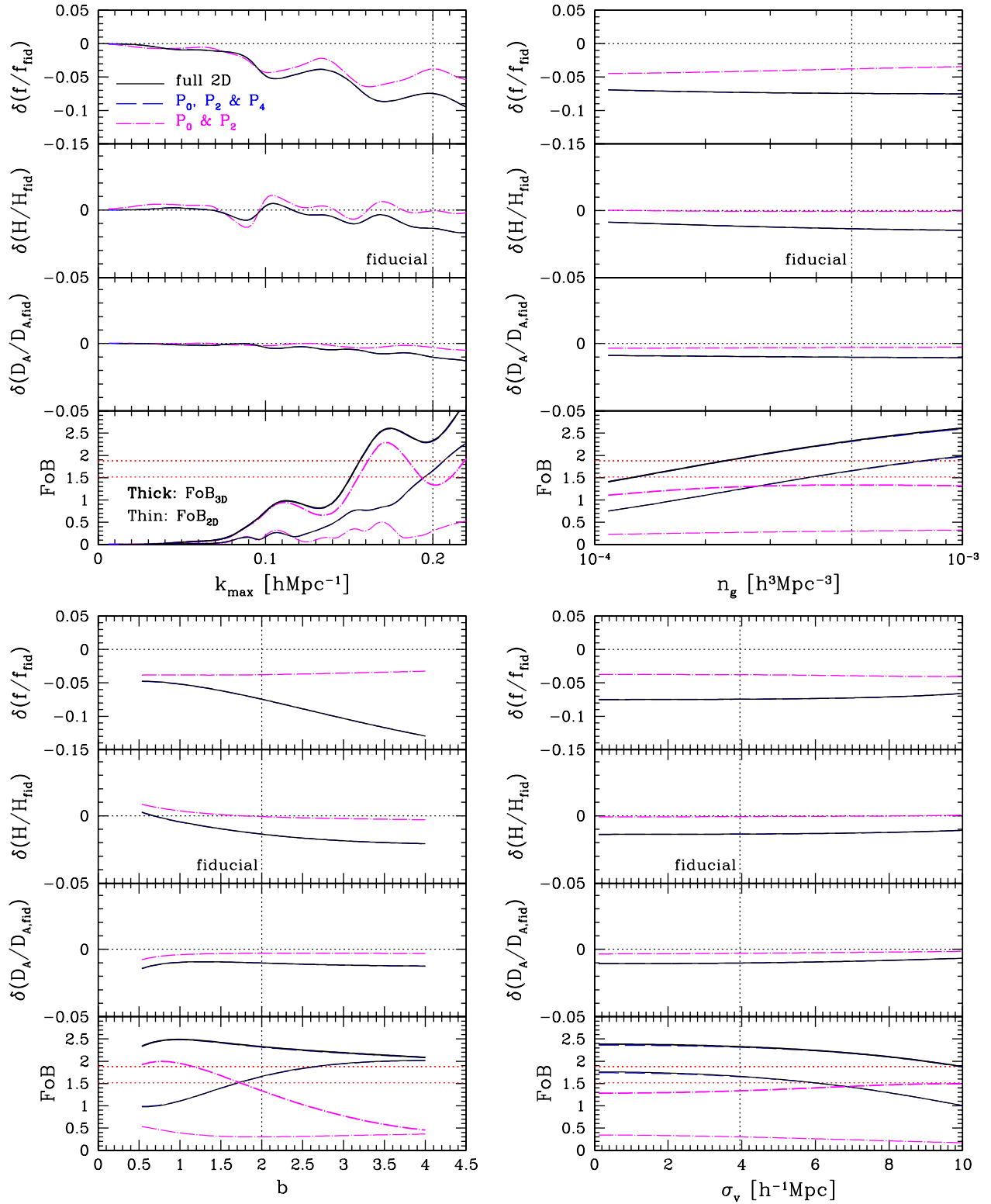
FIG. 5 (color online). Systematic biases for best-fit values of parameters f, D_A and H and figure-of-bias as a function of k_{max} (top left), n_g (top right), b (bottom left), and σ_v (bottom right). These are the estimates adopting the "incorrect" model of redshift-space power spectrum, in which we ignore the small correction terms, A and B. In the bottom plot of each panel, thick and thin lines, respectively, show the FoB in three and two-dimensions, i.e., (D_A, H, f) and (D_A, H). The dotted lines indicate the 1-σ significance of the deviation relative to the statistical error. Note that the shift of the best-fit parameters remains unchanged irrespective of the survey volume V_s, while the FoB given here represents the specific results with the survey volume $V_s = 4h^{-3}$ Gpc^3. The fiducial values of the model parameters used in the calculation are the same as in Fig. 3 (indicated by vertical dotted lines), except for the parameter along the horizontal axis.

above definition, the FoB squared simply reflects the $\Delta\chi^2$ for the true values of the parameters relative to the biased estimate of the best-fit values [53]. Thus, in the cases with three parameters, if the FoB exceeds 1.88 (indicated by the red, thick dotted lines), the true values of the parameters would go outside the 1-σ (68%C.L.) error ellipsoid of the biased confidence region. Notice that the shift of best-fit parameters remains unchanged irrespective of the survey volume V_s, while the FoB is proportional to $V_s^{1/2}$.

Figure 5 shows that the biases in the distance information, δD_A and δH, are basically small and reach 1–2% at most, but the bias in the growth-rate parameter, δf, is rather large. Hence, the behaviors of the FoBs indicated by the thick lines are mostly dominated by the error and bias in the growth-rate parameter. As a result, for some ranges of parameters, the expected FoB using the full-shape information (black solid, labeled as "full 2D") tends to exceed the critical value, 1.88. This is true even if we marginalize over f and just focus on the distance information D_A and H, depicted as thin lines in the lowest panels (labeled as 'FoB$_{2D}$'). Note that in the case of two parameters, the true values of D_A and H are ruled out at the 1-σ level if the FoB exceeds 1.52 (red, thin dotted lines).

On the other hand, if we use the information obtained only from the monopole and quadrupole spectra (magenta, dash-dotted lines), the systematic biases are significantly reduced, and the resultant FoBs are well within the critical values except for unrealistic cases with a large σ_v or antibias $b \lesssim 1$. If we are just interested in D_A and H marginalized over f, the FoB becomes substantially smaller, and would be far below the critical value 1.52, even for a large galaxy survey with $V_s \gtrsim 4h^{-3}$ Gpc^3. Therefore even the partial information from the monopole and quadrupole spectra is helpful and rather robust against the systematic biases than the full 2D information. Although the figure-of-merit for the constraints on D_A, H and f would be degraded, the reduction of FoM is at most a factor of ~0.6, which can be improved to ~0.8 for highly biased objects (see Fig. 3).

Finally, there are several interesting points to be noted. One is the oscillatory behavior of the systematic biases and FoB shown in the top left panel. This originates from the acoustic structure of the power spectrum, and the result suggests that the bias in the growth-rate parameter δf is sensitively affected by the BAO measurement. Another noticeable feature is the suppression of the FoB in the case of three parameters using the monopole and quadrupole spectra, which appears at a larger value of the galaxy bias b (thick, dash-dotted line in bottom left panel). This is presumably due to the fact that, as the clustering bias increases, the systematic bias for the growth-rate parameter tends to be slightly reduced, while the constraint on the growth-rate parameter becomes gradually weaker. A similar trend also appears in the case using the full 2D spectrum, but the suppression is rather small and the FoB never

falls below the critical value, 1.88. This is because the biased estimate of the growth-rate parameter, δf, significantly deviates from the fiducial value, as opposed to the case using monopole and quadrupole spectra.

2. Systematic biases from incorrect prior information

So far, we have assumed that the underlying cosmological parameters necessary to compute the redshift-space power spectrum are known *a priori* from CMB observations such as PLANCK. However, even precision CMB measurements produce some uncertainties in the cosmological parameters due to parameter degeneracies. This can give an incorrect theoretical template for the redshift-space power spectrum, leading to biased estimates of D_A, H, and f.

Figure 6 quantifies the size of systematic biases and FoB arising from the incorrect assumptions for cosmological parameters. Here, we especially focus on the parameters
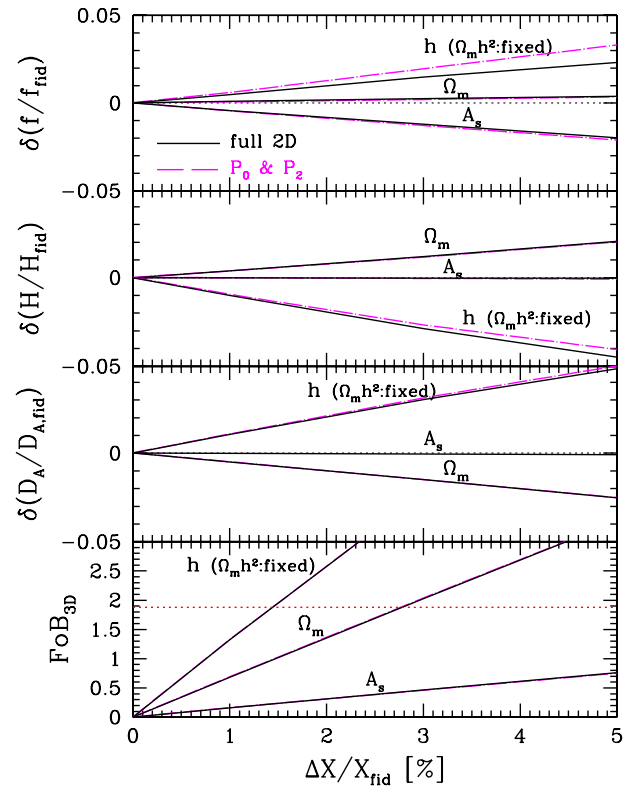

FIG. 6 (color online). Systematic biases for the best-fit values of the parameters f, D_A and H, and FoB for these three parameters (from top to bottom), adopting the incorrect prior information for cosmological parameters in computing the template power spectrum; $X = A_s$, Ω_m, and h ($\Omega_m h^2$: fixed). The results are plotted against the fractional difference between the correct and incorrect values of each cosmological parameters, $\Delta X/X_{fid}$. Solid and dashed lines represent the results from a full 2D power spectrum and partial information with monopole and quadrupole spectra, respectively. Note that in the bottom panel, the horizontal dotted lines indicate the 1-σ significance of the deviation relative to the statistical error.

A_s, $\Omega_{\rm m}$, and h fixing $\Omega_{\rm m}h^2$ constant, and plot the sensitivity of the systematic biases to the variation of those parameters. Note that in computing the power spectrum, we strictly assume the flat cosmological model and the model of redshift distortion (15) as the fiducial power spectrum template.

Compared to the results in Sec. IV C 1, the systematic bias in the growth-rate parameter is relatively small, while the significance of the biases in the acoustic-scale information is increased. That is, the best-fit values of the parameters D_A and H are rather sensitive to the precision of the prior information in the power spectrum template. A noticeable point is that this is true irrespective of the choice of the template power spectra used in the parameter estimation (i.e., full 2D spectrum or combination of P_0 and P_2). As a result, a percent-level precision is generally required for the prior information of cosmological parameters, except for the scalar spectral amplitude, A_s. Through the nonlinear clustering and/or redshift distortion, a small change in A_s alters the power spectrum shape, and it can potentially affect the acoustic-scale and the clustering anisotropies. However, at $z = 1$, the nonlinear effects on the scales of our interest, $k \lesssim 0.2h$ Mpc^{-1}, is rather mild, and the resultant impact on the acoustic-scale measurement is extremely small. Hence, for a typical survey volume of stage-III-class survey with $V_s \sim 4h^{-3}$ Gpc^3, no appreciable systematic bias might be produced from the incorrect prior assumption on A_s.

V. SUMMARY

In this paper, we have studied the cosmological constraints from the anisotropic BAOs based on the multipole expansion of the redshift-space power spectrum. We have derived several formulae for the Fisher analysis using the multipole power spectra; Eqs. (7) and (8) for the Fisher matrix, and Eqs. (11) and (12) for the estimation of systematic biases. We then consider a hypothetical galaxy survey of $V_s = 4h^{-3}$ Gpc^3 and $z = 1$, and discuss the potential power of using the lower-multipole spectra to obtain cosmological constraints, particularly focusing on the parameters D_A, H and f.

Compared to the analysis with the full 2D power spectrum, the partial information from the monopole and quadrupole power spectra generally degrades the constraints on D_A, H, and f. Typically, the constraint is degraded by a factor of ~ 1.3 for each parameter. The interesting finding is that adding the information from hexadecapole spectra (P_4) to that from the monopole and quadrupole spectra greatly improves the constraints, and the resultant constraints would become almost comparable to those expected from the full 2D power spectrum (see Fig. 3). Note also that the situation would be relatively improved depending on the properties of galaxy samples, and for highly biased galaxy samples with $b \sim 4$, the total power of the constraints defined by the figure-of-merit [Eq. (19)]

can reach $\sim 80\%$ of the one expected from the full 2D power spectrum.

We have also investigated the impacts of systematic biases on the best-fit values of D_A, H and f. The incorrect model of redshift distortion tends to produce a large systematic bias in the growth-rate parameter, and the size of biases would be rather significant for the analysis with the full 2D spectrum. An interesting suggestion is that the situation would be greatly relaxed if we only use the combination of monopole and quadrupole spectra, and the estimated value of figure-of-bias defined by Eq. (21) is mostly below the critical value for stage-III-class surveys (Fig. 5). In this respect, the analysis with partial information from the monopole and quadrupole may still be helpful in cross-checking the results derived from the full 2D power spectrum. On the other hand, wrong prior assumption of cosmological parameters in computing the template power spectrum severely affects the acoustic-scale determination, and a percent-level precision is required for the prior information in order to avoid large systematic biases on D_A and H (Fig. 6). This is true irrespective of the choice of template power spectra used in the analysis.

Finally, we note that the assumptions and situations considered in the paper are somewhat optimistic or too simplistic, and a more careful study is needed for a quantitative parameter forecast. One critical aspect is the modeling of the galaxy power spectrum. In reality, the assumption of linear and deterministic galaxy biasing is idealistic, and the scale-dependence or nonlinearity/stochasticity of the galaxy biasing should be consistently incorporated into the theoretical template of the redshift-space power spectrum. Although this is a tiny effect for the scale of our interest, the distance information, D_A and H, is rather sensitive to a slight modification of the acoustic structure in the power spectrum, and results in this paper might be somehow changed. A more elaborate modeling for the power spectrum is thus quite essential.

[1] D. J. Eisenstein *et al.* (SDSS), Astrophys. J. **633**, 560 (2005).

[2] W. J. Percival *et al.*, Mon. Not. R. Astron. Soc. **381**, 1053 (2007).

[3] W. J. Percival *et al.*, Mon. Not. R. Astron. Soc. **401**, 2148 (2010).

[4] C. Alcock and B. Paczynski, Nature (London) **281**, 358 (1979).

[5] H.-J. Seo and D. J. Eisenstein, Astrophys. J. **598**, 720 (2003).

[6] C. Blake and K. Glazebrook, Astrophys. J. **594**, 665 (2003).

[7] M. Shoji, D. Jeong, and E. Komatsu, Astrophys. J. **693**, 1404 (2009).

[8] N. Padmanabhan and M. J. White, Phys. Rev. D **77**, 123540 (2008).

[9] E. V. Linder, Astropart. Phys. **29**, 336 (2008).

[10] L. Guzzo *et al.*, Nature (London) **451**, 541 (2008).

[11] K. Yamamoto, T. Sato, and G. Huetsi, Prog. Theor. Phys. **120**, 609 (2008).

[12] Y.-S. Song and W. J. Percival, J. Cosmol. Astropart. Phys. 10 (2009) 004.

[13] D. Schlegel, M. White, and D. Eisenstein (with input from the SDSS-III), arXiv:0902.4680.

[14] G. J. Hill *et al.*, Astron. Soc. Pac. Conf. Ser. **399**, 115 (2008).

[15] J. P. Beaulieu *et al.*, arXiv:1001.3349.

[16] N. Gehrels, arXiv:1008.4936.

[17] H.-J. Seo and D. J. Eisenstein, Astrophys. J. **665**, 14 (2007).

[18] M. White, Y.-S. Song, and W. J. Percival, Mon. Not. R. Astron. Soc. **397**, 1348 (2009).

[19] Throughout the paper, we work with the distant-observer approximation, and neglect the angular dependence of the line-of-sight direction, relevant for the high-redshift galaxy surveys.

[20] T. Okumura *et al.*, Astrophys. J. **676**, 889 (2008).

[21] R. Takahashi *et al.*, Astrophys. J. **700**, 479 (2009).

[22] A. Cabre and E. Gaztanaga, Mon. Not. R. Astron. Soc. **393**, 1183 (2009).

[23] N. Kaiser, Mon. Not. R. Astron. Soc. **227**, 1 (1987), [http://adsabs.harvard.edu/abs/1987MNRAS.227....1K].

[24] A. J. S. Hamilton, Astrophys. J. **385**, L5 (1992).

[25] A. J. S. Hamilton, arXiv:astro-ph/9708102.

[26] D. Tocchini-Valentini, M. Barnard, C. L. Bennett, and A. S. Szalay, arXiv:1101.2608.

[27] E. Komatsu *et al.* (WMAP), Astrophys. J. Suppl. Ser. **180**, 330 (2009).

[28] K. Yamamoto, Astrophys. J. **595**, 577 (2003).

[29] M. Tegmark, Phys. Rev. Lett. **79**, 3806 (1997).

[30] H. A. Feldman, N. Kaiser, and J. A. Peacock, Astrophys. J. **426**, 23 (1994).

[31] K. Yamamoto, M. Nakamichi, A. Kamino, B. A. Bassett, and H. Nishioka, Publ. Astron. Soc. Jpn. **58**, 93 (2006), [http://pasj.asj.or.jp/v58/n1/580114/580114-frame.html].

[32] Here, we use the standard notation for the multipole expansion of redshift power spectra given by (1), which differs from the definition of Ref. [31]

[33] S. Saito, M. Takada, and A. Taruya, Phys. Rev. D **80**, 083528 (2009).

[34] A. Taruya, T. Nishimichi, and S. Saito, Phys. Rev. D **82**, 063522 (2010).

[35] R. Scoccimarro, M. Zaldarriaga, and L. Hui, Astrophys. J. **527**, 1 (1999).

[36] R. Takahashi *et al.*, Astrophys. J. **726**, 7 (2011).

[37] M. Takada and B. Jain, Mon. Not. R. Astron. Soc. **395**, 2065 (2009).

[38] A. Kiessling, A. N. Taylor, and A. F. Heavens, arXiv:1103.3245.

[39] M. C. Neyrinck and I. Szapudi, Mon. Not. R. Astron. Soc. **384**, 1221 (2008).

[40] R. Scoccimarro, Phys. Rev. D **70**, 083007 (2004).

[41] The definition of velocity dispersion $\sigma_{\rm v}$ adopted in this paper differs from the one commonly used in the literature by a factor of f, but coincides with those in Refs. [34,40].

[42] A. Taruya, T. Nishimichi, S. Saito, and T. Hiramatsu, Phys. Rev. D **80**, 123503 (2009).

[43] M. Crocce and R. Scoccimarro, Phys. Rev. D **77**, 023533 (2008).

[44] T. Okumura and Y. P. Jing, Astrophys. J. **726**, 5 (2011).

[45] D. Jeong and E. Komatsu, Astrophys. J. **691**, 569 (2009).

[46] S. Saito, M. Takada, and A. Taruya, Phys. Rev. D **83**, 043529 (2011).

[47] W. E. Ballinger, J. A. Peacock, and A. F. Heavens, Mon. Not. R. Astron. Soc. **282**, 877 (1996), [http://adsabs.harvard.edu/abs/1996MNRAS.282..877B].

[48] H. Magira, Y. P. Jing, and Y. Suto, Astrophys. J. **528**, 30 (2000).

[49] A. J. Albrecht *et al.*, arXiv:astro-ph/0609591.

[50] A. Taruya and T. Hiramatsu, Astrophys. J. **674**, 617 (2008).

[51] The Planck Collaboration arXiv:astro-ph/0604069.

[52] S. Joudaki, A. Cooray, and D. E. Holz, Phys. Rev. D **80**, 023003 (2009).

[53] C. Shapiro, Astrophys. J. **696**, 775 (2009).

[54] D. J. Eisenstein and W. Hu, Astrophys. J. **496**, 605 (1998).